

## REPORT No. 613

# THE VARIATION WITH REYNOLDS NUMBER OF PRESSURE DISTRIBUTION OVER AN AIRFOIL SECTION

By ROBERT M. PINKERTON

### SUMMARY

Pressures were simultaneously measured at 54 orifices distributed over the midspan section of a 5- by 30-inch rectangular model of the N. A. C. A. 4412 airfoil in the variable-density tunnel. These measurements were made at 17 angles of attack from  $-20^\circ$  to  $30^\circ$  for eight values of the effective Reynolds Number from approximately 100,000 to 8,200,000. Accurate data were thus obtained for studying the variation of pressure distribution with Reynolds Number.

These results on the N. A. C. A. 4412 section indicate that the pressure distribution is practically unaffected by changes in Reynolds Number except where separation is involved.

### INTRODUCTION

The need for pressure-distribution data over an airfoil section and the methods of obtaining those data are discussed in detail in reference 1. Briefly, such data provide directly the load distributions required for design purposes and, in addition, the comparison of measured pressures with those computed from potential-flow (nonviscous fluid) theory provides a means of studying the effects of viscous forces on the flow about the airfoil section. Moreover, with the wide range of Reynolds Numbers in use, it is desirable to know how the pressure distribution varies with Reynolds Number. Indications of changes in the character of the flow with Reynolds Number may also be deduced from the measured pressure distributions.

An extensive investigation of the pressure distribution over one section of the N. A. C. A. 4412 airfoil has been carried out in the variable-density wind tunnel. The purpose was twofold: First, to provide adequate experimental data to compare with theoretical results; and second, to study the variations with Reynolds Number. Reference 1 presents the most important phase of the investigation and is divided into two parts. The first part gives a detailed discussion of the experimental technique and a presentation of the results at the highest Reynolds Number. In the second part a comparison is made of experimental with calculated pressure distributions, and a modified method of calcu-

lation, giving more accurate results than those obtained by the usual potential-flow method, is developed.

The present report presents the complete experimental data for the same airfoil at eight values of the Reynolds Number and an analysis of the variations with Reynolds Number.

### APPARATUS AND TESTS

The model used in this pressure-distribution investigation was a standard duralumin airfoil of N. A. C. A. 4412 section with a span of 30 inches and a chord of 5 inches. Pressure orifices, placed in two rows one-quarter inch apart, were located at 54 stations around the midspan section as given in table I. In order to evaluate the pressure force parallel to the chord, a relatively large number of orifices were located at the nose of the airfoil (fig. 1); well-defined distributions of pressure along a normal to the chord were thus assured.

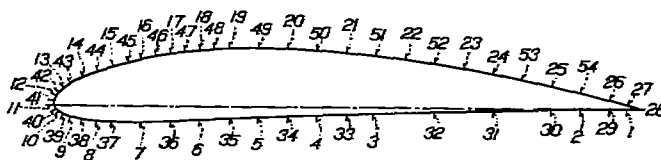


FIGURE 1.—Distribution of pressure orifices about the N. A. C. A. 4412 profile.

Pressures were measured at 17 angles of attack from  $-20^\circ$  to  $30^\circ$  to obtain data throughout the range including the stall at both positive and negative angles of attack. These measurements were made at eight values of the Reynolds Number obtained by varying the density of the air in the tank that houses the tunnel (reference 2). Values of the effective Reynolds Number, obtained by multiplying the test Reynolds Number by the turbulence factor 2.64 (reference 3), and the corresponding tank pressures are given below.

Tank pressure (atmospheres):	Effective Reynolds Number
1/4	0.10 × 10 <sup>6</sup>
1/2	.24
1	.45
2	.90
4	1.80
8	3.40
15	6.30
21	8.20

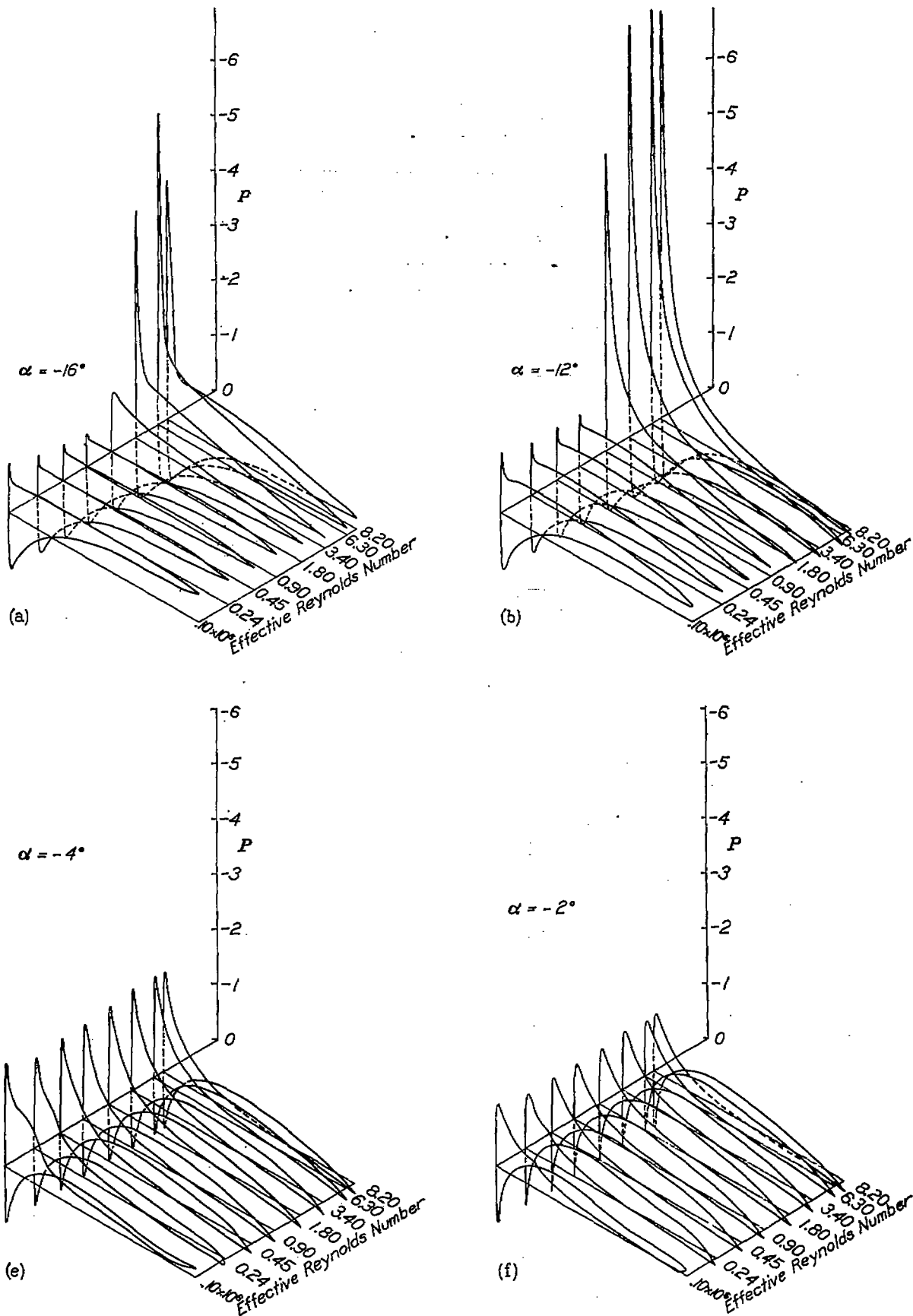


FIGURE 2(a) to 2(p).—Pressure-distribution diagrams for the N. A. O. A. 4412 airfoil.

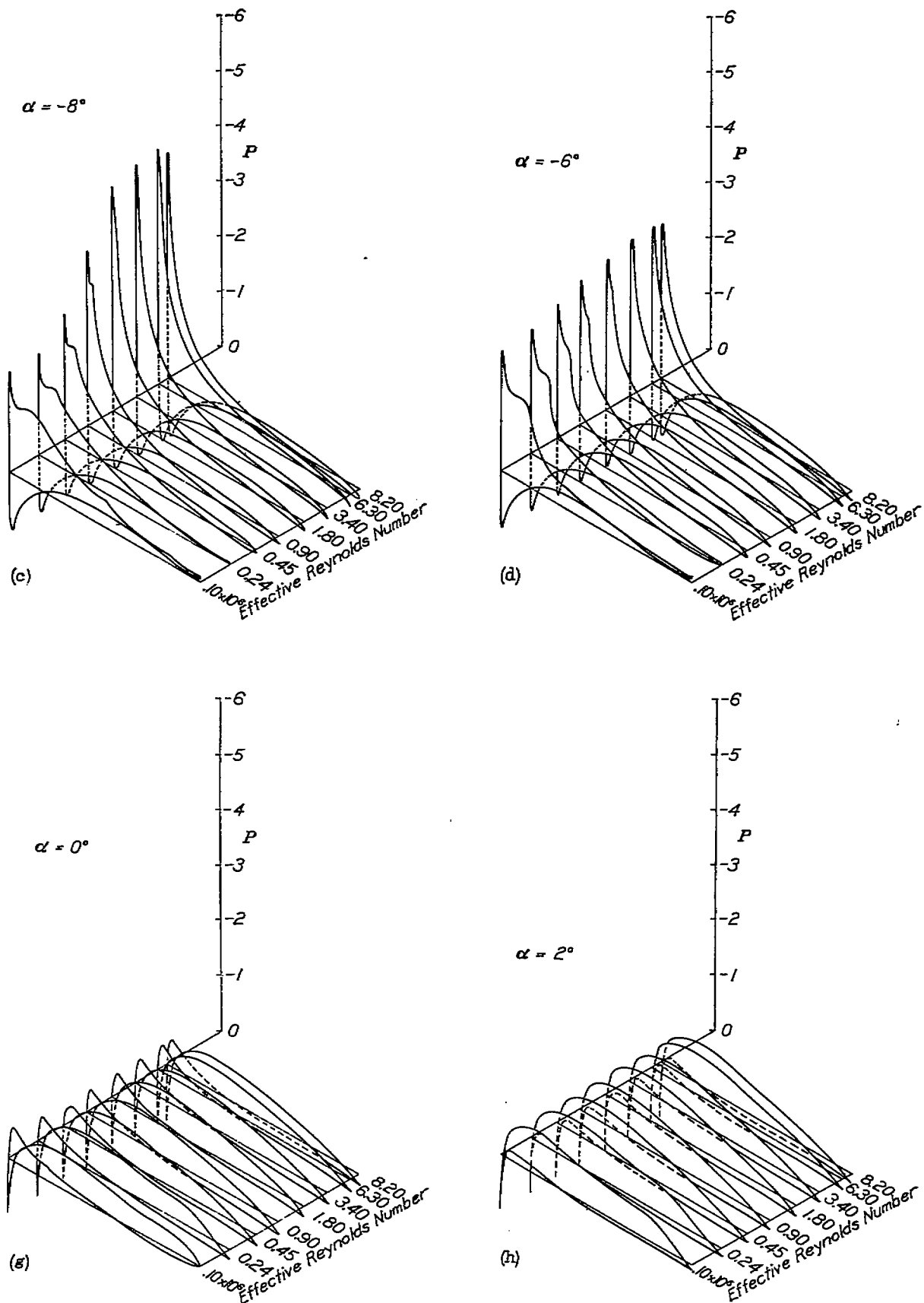


FIGURE 2.—Continued. Pressure-distribution diagrams for the N. A. C. A. 4412 airfoil.

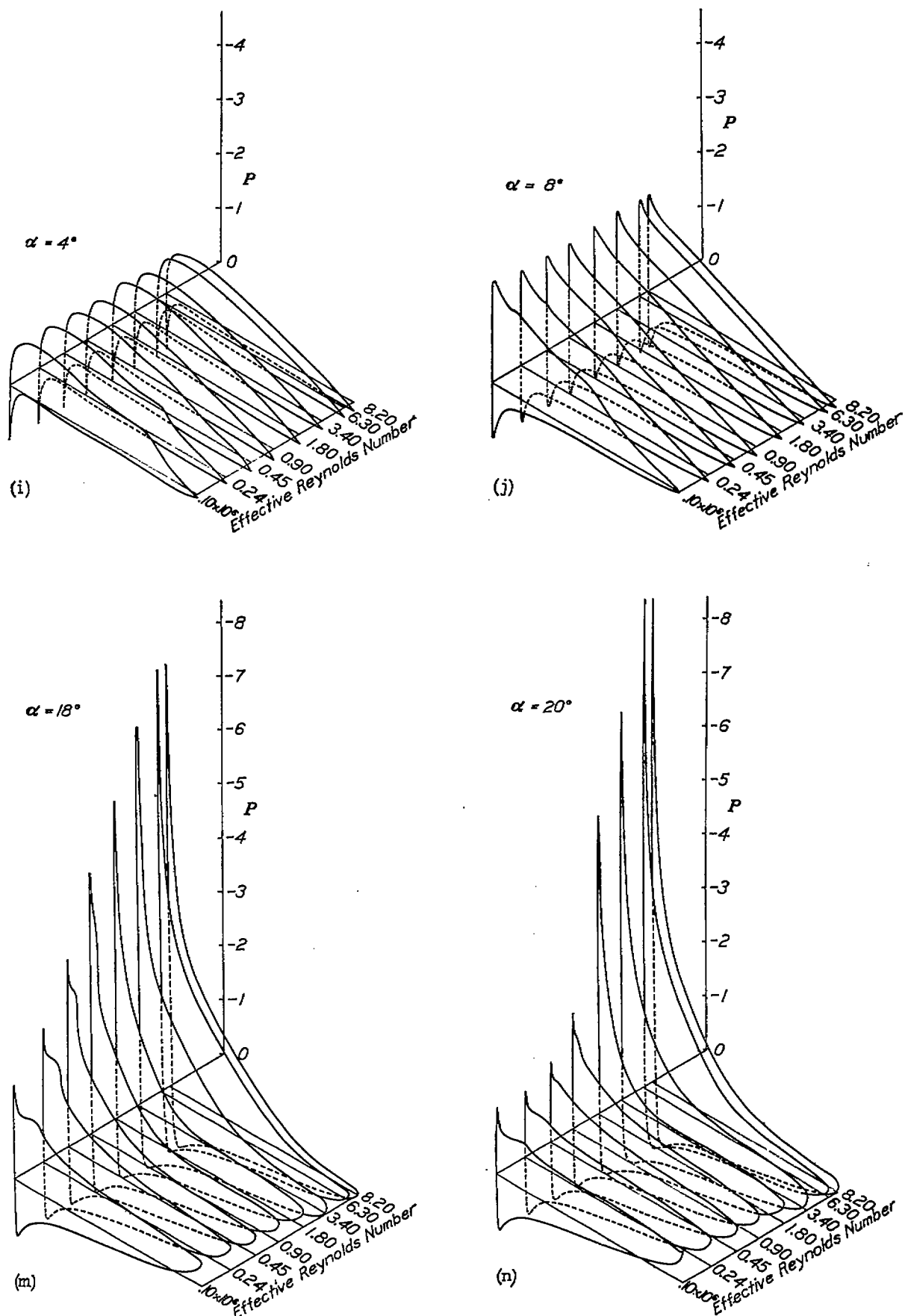


FIGURE 2.—Continued. Pressure-distribution diagrams for the N. A. C. A. 4412 airfoil.

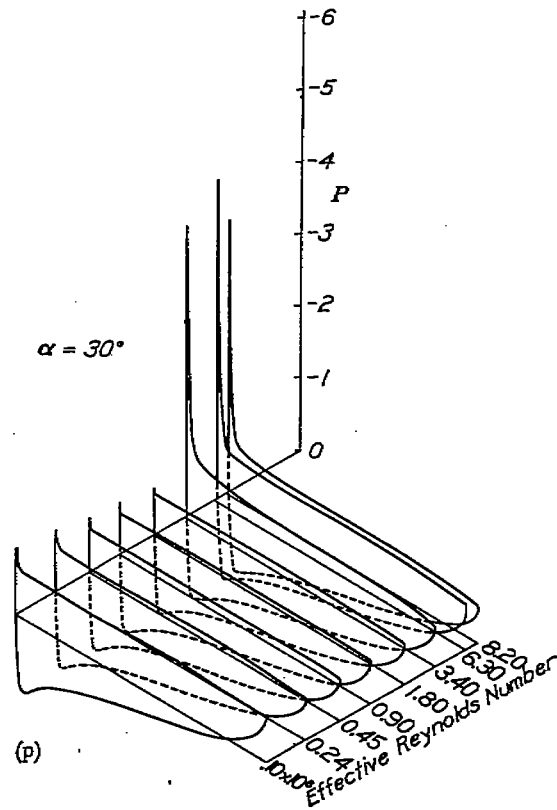
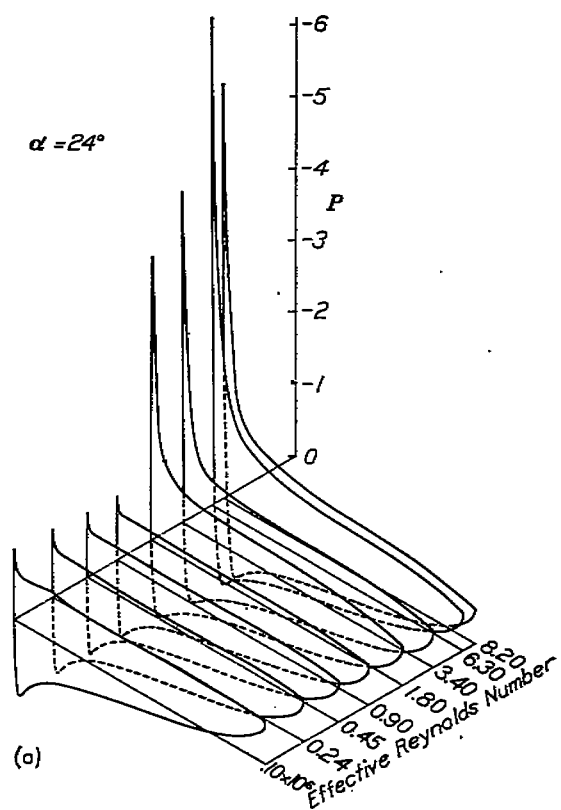
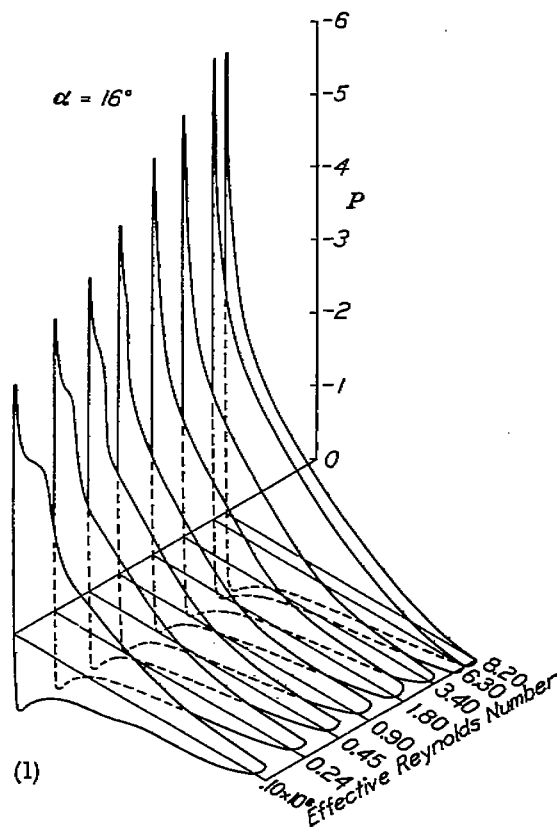
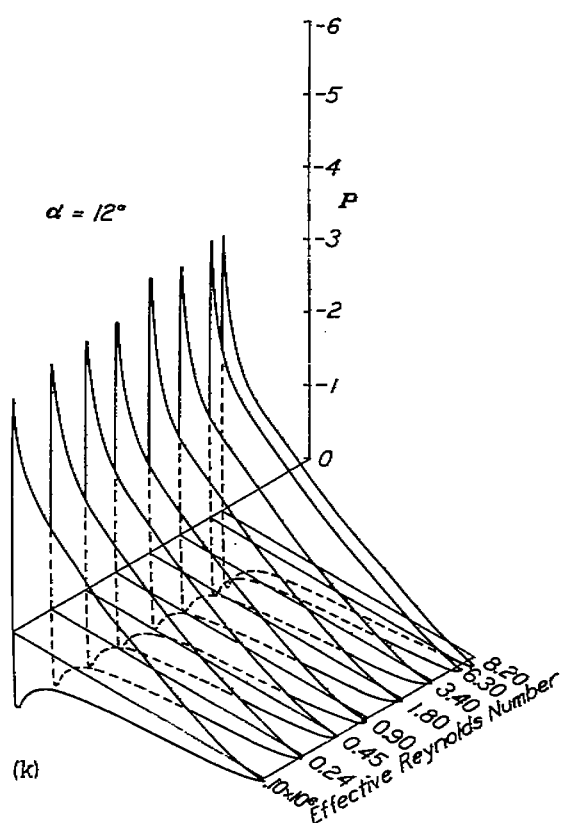


FIGURE 2.—Continued. Pressure-distribution diagrams for the N. A. C. A. 4412 airfoil.

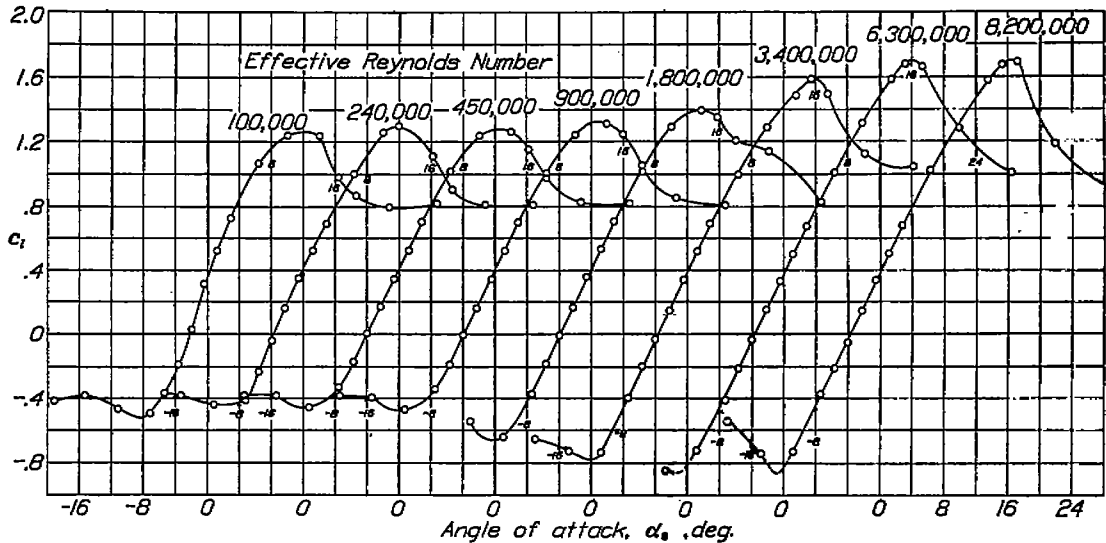


FIGURE 3.—Lift curves for the N. A. C. A. 4412 airfoil at several values of the Reynolds Number.

In order to keep the pressure measurements as accurate as possible, it was necessary to obtain large deflections of the manometer liquids, which was accomplished by using three liquids of widely different specific gravities.

Liquid:	Specific gravity
Mercury.....	13.6
Tetrabromoethane.....	3.0
Alcohol.....	.9

The proper choice of the angle of attack and Reynolds Number groups and of the liquid enabled the use of large and comparable deflections throughout all conditions of the investigation. Repeat tests using the same and different manometer liquids provided data on the precision of the tests.

The values of the pressure coefficient  $P = (p - p_\infty)/q$  at each orifice on the airfoil and for all angles of attack are tabulated in table I; the table is divided into sections (a) to (h), each section comprising the data for one value of the Reynolds Number. The pressures  $p$  and  $p_\infty$  are, respectively, the pressures at the orifice and in the undisturbed stream.

As in reference 1, the data were reduced to the following section coefficients for the midspan section of the airfoil.

$$c_n = \frac{1}{c} \int P dx$$

$$c_c = \frac{1}{c} \int P dy$$

$$c_{m_{c/4}} = \frac{1}{c^2} \left[ \int P (c/4 - x) dx + \int P y dy \right]$$

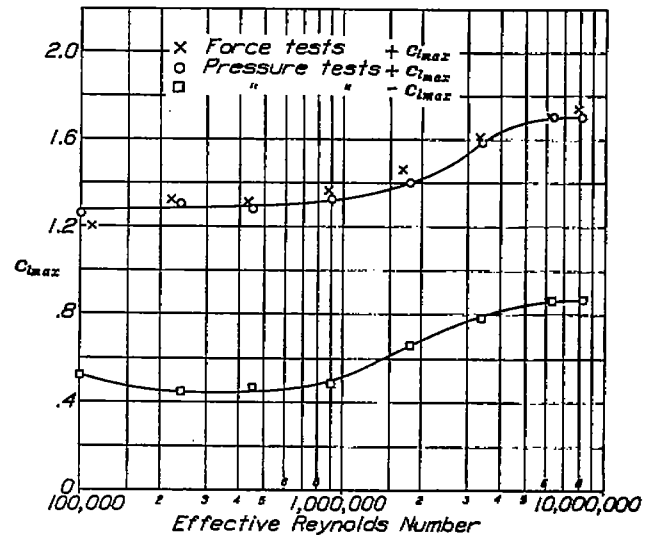
where  $c_n$  is the section normal-force coefficient.

$c_c$ , section chord-force coefficient.

$c_{m_{c/4}}$ , section pitching-moment coefficient.

Lift coefficients were obtained from the pressure measurements by the following equation:

$$c_l = c_n \cos \alpha - c_c \sin \alpha$$

FIGURE 4.—Variation of  $C_{l_{max}}$  with Reynolds Number.

The effective angle of attack is given by

$$\alpha_0 = \alpha - \alpha_t$$

and the induced angle of attack of the midspan section by

$$\alpha_t = 1.584 c_l$$

where  $\alpha$  is the geometric angle of attack measured from the mean direction of flow in the tunnel.

$\alpha_t$ , the angle that the flow in the region of the airfoil section makes with the direction of the undisturbed flow.

Values of  $c_n$ ,  $c_c$ ,  $c_{m_{c/4}}$ ,  $c_l$ ,  $\alpha_t$ , and  $\alpha_0$  for the 17 values of  $\alpha$  are given in table II; the sections (a) to (h) correspond to the respective Reynolds Numbers of table I(a) to (h).

Isometric plots of normal pressure against position along the chord are presented in figure 2, one set of plots containing the pressures for the eight Reynolds Numbers at each angle of attack. The effect of Reynolds Number on the lift characteristics is shown in figures 3 and 4.

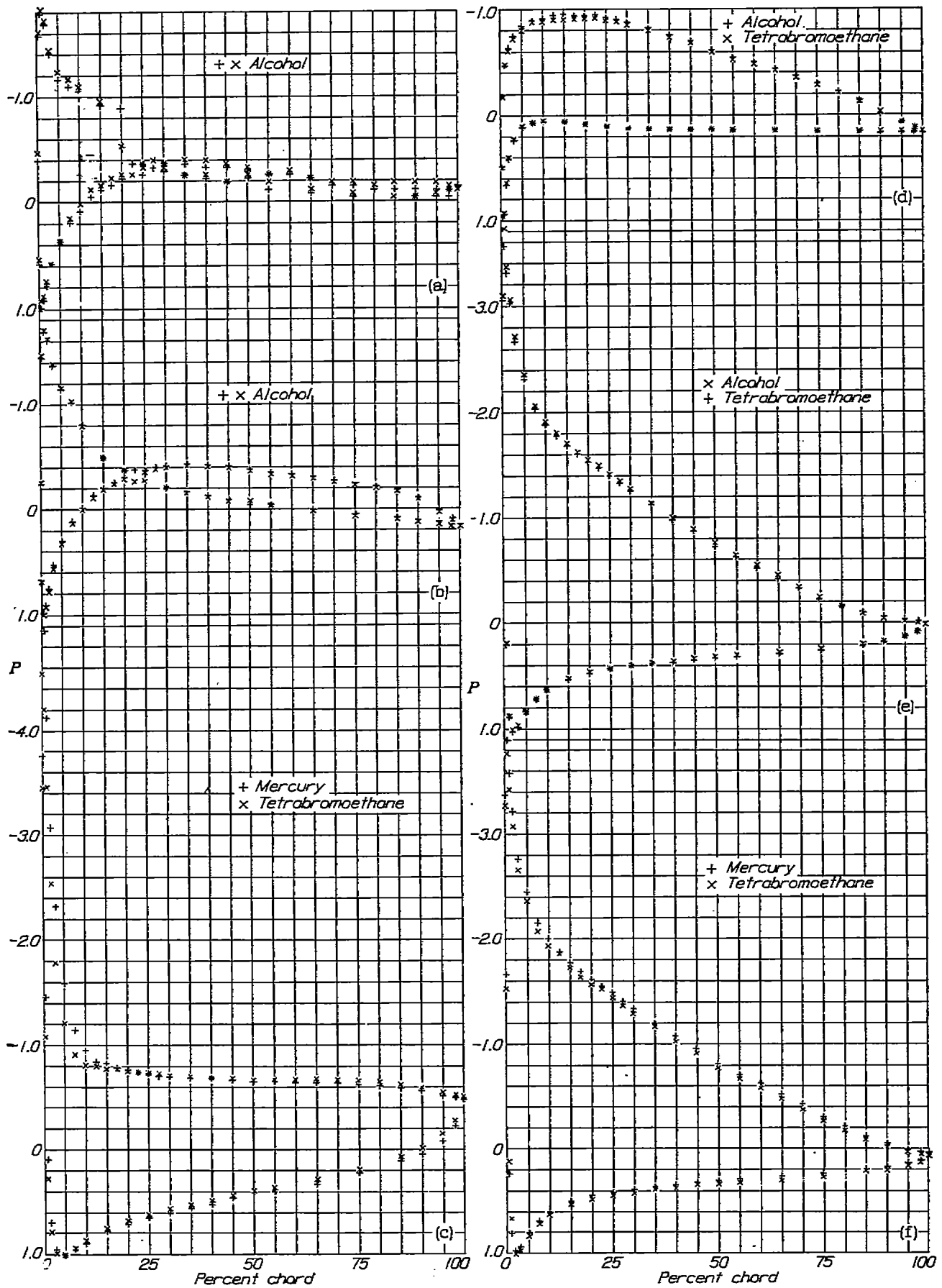


FIGURE 5.—Pressure-distribution diagrams from repeat tests at various angles of attack and values of the Reynolds Number. Values indicated by X are also given in table I.

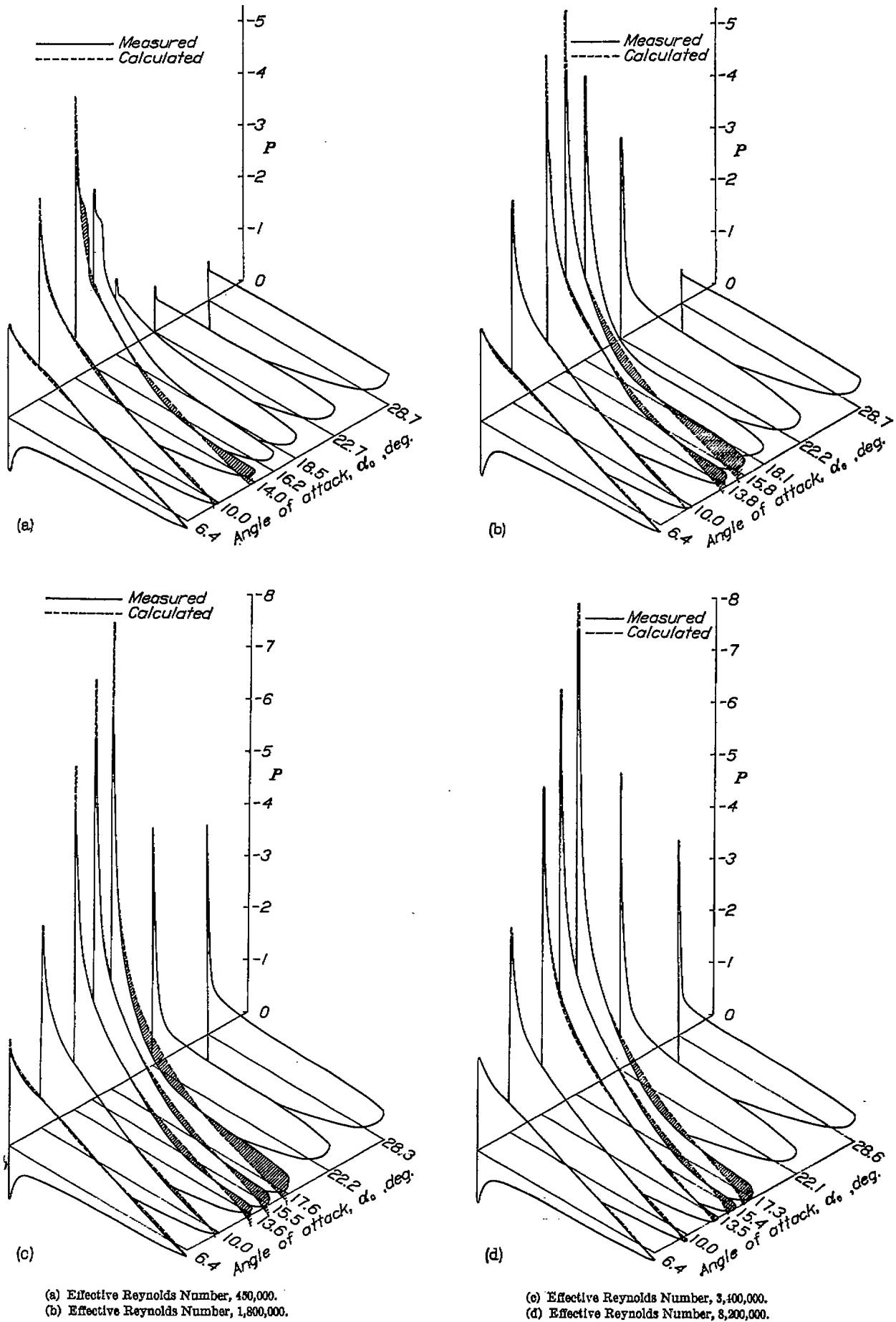


FIGURE 6.—Pressure-distribution diagrams showing the spread of separation at four values of the Reynolds Number.



## PRECISION

The precision of the pressure measurements at Reynolds Numbers other than that for the data published in reference 1 is indicated by the diagrams given in figure 5. At the lowest Reynolds Number (fig. 5 (a)) the capacity to repeat measured pressures is markedly less than for higher Reynolds Numbers. It should be noted, however, that the precision was good enough to establish the occurrence of the supposedly laminar separation near the leading edge. The precision at Reynolds Numbers corresponding to the atmospheric runs and at higher values is consistently good even when the section has stalled, as in the diagram for  $24^\circ$ .

## DISCUSSION

The general nature of the variation of the pressure distribution with Reynolds Number may be observed by means of the isometric plots in figure 2. At normal angles of attack, where stalling is not involved, the distributions are practically unaffected and hence the modified method of calculation presented in reference 1 is applicable at those attitudes for any Reynolds Number. Differences that do occur in the pressure diagrams are entirely of a local nature; they are probably associated with separation and the changes in the character of the boundary layer as the Reynolds Number is varied.

**Boundary layer and the pressure distribution.**—The formation of the boundary layer due to the viscous forces and the resulting effect on the pressure distribution is discussed in reference 1. A comparison of actual pressures with those computed for a potential, or non-viscous, fluid led to the development of the previously mentioned modified method of calculation, which gives good results at attitudes where separation is not involved.

Separation of the flow from the surface would be expected to be indicated on the pressure diagrams by a region of approximately constant pressures. The start and growth of separation are best observed in figure 6, which presents isometrically the pressure diagrams for an increasing angle-of-attack range. Calculated diagrams obtained by the method of reference 1 for a non-separated viscous flow are superposed for comparison. The differences between the measured and calculated distributions are attributed to separation and hence the shaded area may be considered as a measure of the effect of separation. The inclusion of four groups of diagrams, one for each of four values of the Reynolds Number, provides a means of studying the scale effect on separation phenomena.

The occurrence of separation is markedly affected by changes in the Reynolds Number, as may be seen in figure 6. Moreover, the only observable scale effects on pressure distributions (fig. 2) are probably due to the nature of the separation and the changes in the separa-

tion phenomena experienced with changing Reynolds Number. Most of these changes, of course, appear near either the positive or negative stall but at low Reynolds Numbers (below  $R_c=900,000$  approximately) some effects of separation, even in the low-drag range, are apparent from a careful analysis of the distributions. The presence of some such effects is indicated especially by pressure-drag integrations which, in this range, show a definite increase of drag with decreasing Reynolds Number. These results, however, are not presented as such since pressure-drag determinations are subject to some uncertainty owing to the inherent difficulty in obtaining them. The following analysis is based on changes in pressure distribution occurring near the stall.

A detailed discussion of these phenomena based on analyses of force tests of a large number of airfoils of widely different shapes is given in reference 3. The pressure-distribution data presented herein provide confirmatory and supplementary information for one particular type of airfoil section represented by the N. A. C. A. 4412 airfoil. This airfoil is one of medium thickness and camber producing a fairly gradual stall (type D lift-curve peak, reference 3). The stalling process of this section is a complicated one involving both trailing- and leading-edge types of separation.

At the low Reynolds Number (fig. 6 (a)) separation occurs prior to the stall as indicated in two distinct regions on the N. A. C. A. 4412 airfoil: One in the turbulent boundary layer near the rear of the airfoil, and the other in what is probably the laminar boundary layer near the nose. Instability of the laminar flow after separation results in a breakdown of the smooth laminae into an eddying flow. The scouring action of the eddying flow may then sweep the dead air from the surface and cause the reestablishment of unseparated flow with a turbulent boundary layer instead of the laminar layer. This laminar separation and the subsequent establishment of eddying flow account for the so-called "bubble" of dead air occurring in the flow at the low Reynolds Numbers. The turbulent layer, unable to maintain itself at high angles of attack, starts separating near the trailing edge and spreads forward as the angle is increased until the stall, resulting from the combined laminar and turbulent separations, is reached.

At the highest Reynolds Numbers (fig. 6) marked local laminar separation near the nose of the airfoil is apparently prevented. This prevention is accounted for by a transition from laminar to turbulent flow nearly at the laminar separation point or before the laminar flow has reached separation conditions. A movement forward of this transition region with increasing Reynolds Number has been observed in smoke-flow studies. Moreover, figure 6 indicates that, for the N. A. C. A. 4412 airfoil in the Reynolds Number range included, the separation in the turbulent bound-

ary layer is slightly delayed with increasing Reynolds Number. Hence, at the high Reynolds Number, with possibly a delayed turbulent separation and no marked local laminar separation, the airfoil section increased its lift to a higher angle before stalling than was possible at the low Reynolds Number.

This analysis of the separation phenomena and the changes with Reynolds Number has been confirmed in some respects by measurements in the boundary layer of the N. A. C. A. 4412 airfoil at several values of the Reynolds Number. These data are a part of an N. A. C. A. investigation of boundary-layer phenomena.

Concluding remarks.—The results of this investigation indicate that the pressure distribution except near maximum lift is practically unaffected by changes in the Reynolds Number above a certain critical value, which is below the usual full-scale range. This critical

value is probably the value at which there is no definite local separation.

LANGLEY MEMORIAL AERONAUTICAL LABORATORY,  
NATIONAL ADVISORY COMMITTEE FOR AERONAUTICS,  
LANGLEY FIELD, VA., *July 14, 1937.*

#### REFERENCES

1. Pinkerton, Robert M.: Calculated and Measured Pressure Distributions Over the Midspan Section of the N. A. C. A. 4412 Airfoil. T. R. No. 563, N. A. C. A., 1936.
2. Jacobs, Eastman N., and Abbott, Ira H.: The N. A. C. A. Variable-Density Wind Tunnel. T. R. No. 416, N. A. C. A., 1932.
3. Jacobs, Eastman N., and Sherman, Albert: Airfoil Section Characteristics as Affected by Variations of the Reynolds Number. T. R. No. 586, N. A. C. A., 1937.





















TABLE IIg.—INTEGRATED AND DERIVED CHARACTERISTICS

[N. A. C. A. 4412 airfoil; effective Reynolds Number, 8,300,000]

$\alpha$ (deg.)	$c_n$	$c_o$	$c_{m_{a/l}}$	$c_l$	$\alpha_1$ (deg.)	$\alpha_0$ (deg.)
-20						
-16	-0.869	-0.0497	0.026	-0.849	-1.3	-14.7
-12	-0.712	-0.1245	-0.103	-0.722	-1.1	-10.9
-8	-0.410	-0.0417	-0.069	-0.412	-0.7	-7.3
-6	-0.209	-0.0155	-0.064	-0.210	-0.3	-5.7
-4	-0.036	-0.0029	-0.033	-0.036	0	-4.0
-2	.187	.0118	-0.02	.187	.2	-2.2
0	.333	.0079	-0.01	.333	.5	-0.5
.2	.501	-0.034	-0.07	.500	.8	1.2
.4	.674	-0.055	-0.08	.674	1.1	2.0
.8	1.002	-0.098	-0.080	1.000	1.6	6.4
12	1.300	-0.212	-0.073	1.315	2.1	9.9
16	1.550	-0.3410	-0.064	1.534	2.5	13.5
18	1.633	-0.4020	-0.067	1.678	2.7	15.3
20	1.605	-0.4425	-0.061	1.661	2.6	17.4
24	1.300	-0.2329	-0.143	1.293	2.0	23.0
30	1.111	-0.1019	-0.171	1.014	1.6	28.4

TABLE IIIh.—INTEGRATED AND DERIVED CHARACTERISTICS

[N. A. C. A. 4412 airfoil; effective Reynolds Number, 8,200,000]

$\alpha$ (deg.)	$c_n$	$c_o$	$c_{m_{a/l}}$	$c_l$	$\alpha_1$ (deg.)	$\alpha_0$ (deg.)
-20	-0.592	0.0318	0.030	-0.545	-0.9	-19.1
-16	-0.767	-0.0170	-0.035	-0.742	-1.2	-14.8
-12	-0.722	-0.1264	-0.02	-0.732	-1.2	-10.8
-8	-0.372	-0.0445	-0.036	-0.374	-0.8	-7.4
-6	-0.210	-0.0161	-0.026	-0.211	-0.8	-5.7
-4	-0.026	-0.0043	-0.025	-0.026	0	-4.0
-2	.146	.0107	-0.022	.146	.2	-2.2
0	.338	.0098	-0.021	.338	.5	-0.5
.2	.501	-0.034	-0.067	.501	.8	1.2
.4	.677	-0.058	-0.067	.677	1.1	2.0
.8	1.020	-0.1003	-0.084	1.024	1.6	6.4
12	1.275	-0.2043	-0.074	1.289	2.0	10.0
16	1.548	-0.3357	-0.068	1.579	2.5	13.5
18	1.626	-0.4040	-0.063	1.671	2.6	15.4
20	1.640	-0.4374	-0.060	1.630	2.7	17.3
24	1.312	-0.2328	-0.141	1.312	2.0	22.1
30	1.009	-0.0776	-0.146	.913	1.4	28.6